Progress In Electromagnetics Research, PIER 80, 477–497, 2008

THE *M-DSO-ESPRIT* METHOD FOR MAXIMUM LIKELIHOOD *DOA* ESTIMATION

L. Lizzi, F. Viani, M. Benedetti, P. Rocca, and A. Massa

Department of Information and Communication Technology
University of Trento
Via Sommarive 14, Trento 38050, Italy

Abstract—The estimation of the directions-of-arrival (DoAs) of multiple signals is a topic of great relevance in smart antenna synthesis and signal processing applications. In this paper, a memory-based method is proposed to compute the maximum likelihood (ML) DoA estimates. Such a conceptually-simple technique is based on the data-supported optimization (DSO) and the estimation of signal parameters via rotational invariance technique ($ESPRIT$), but fully exploits a memory mechanism for improving the estimation accuracy especially when dealing with critical scenarios characterized by low signal-to-noise ratios (SNR) or/and small number of snapshots. Simulation results assess the potentialities and limitations of the proposed approach that favorably compares with state-of-the-art methods.

1. INTRODUCTION

Smart antennas are a challenging research topic in electromagnetics and wireless communications. The main reason for the growing interest about such an issue when dealing with multi-users communication systems, mainly lies in the need of adaptively facing with unknown time-varying scenarios [1–3]. In general, smart systems consist of an array of radiating elements able to steer the main lobe beam towards the desired signal [4–6] and to locate suitable nulls of the radiation pattern in the directions of the interferences [7–9]. Accordingly, a relevant step for building a smart receiver is concerned with the estimation of the directions of arrival (DoAs) of the received signals. Towards this end, various techniques have been developed not only for wireless communications, but also in various applications ranging from radar [10–12] to sonar [13] and speech processing [14].

The maximum likelihood (ML) estimator has been largely used in direction finding problems because of its capability of reaching, asymptotically and under regularity conditions, the Cramer-Rao Bound (CRB) [15]. Unfortunately, it is characterized by an intrinsic complexity arising from the multi-modal nature of the likelihood function (LF) and by the high computational load of the involved multivariate nonlinear maximization problem [16–18]. Therefore, other sub-optimal approaches have been proposed in order to reach a suitable trade-off between estimation accuracy and complexity.

Concerning learning-by-examples (LBE) techniques, some methods based on the use of radial-basis functions (RBF) [19, 20] and support vector machines [21–23] have been efficiently applied to single- and multiple-source direction finding, as well.

Unlike LBE techniques that need of a learning phase for training the underlying network architecture, super-resolution approaches directly process the received signals without any off-line pre-processing or training. In such a framework, the multiple signal classification method ($MUSIC$) [24] is an eigenstructure-based direction finding technique that employs the noise-subspace eigenvectors of the data correlation matrix for determining a null spectrum, whose minima are iteratively computed to yield the DoA estimates. Although it asymptotically converges to the CRB [25] for an increasing number of snapshots, the standard implementation of $MUSIC$ still implies high computational and storage costs [26] because of the exhaustive search extended to the whole set of steering vectors. As far as uniform linear arrays (ULAs) are concerned, the so-called $ROOT\text{-}MUSIC$ [27] version can be profitably used by solving a polynomial rooting problem, thus improving the computational performances of the $MUSIC$ algorithm [28].

Likewise $MUSIC$, the estimation of signal parameters via rotational invariance technique ($ESPRIT$) [29] is a vector subspace-based methodology that, instead of identifying the spectral peaks, directly determines the DoAs by exploiting the *rotational invariance* of the underlying signal subspace induced by the *translational invariance* of the sensors array. Since the $ESPRIT$ complexity strictly depends on the number of sensors, faithful estimates and a reduced computational burden can be achieved dealing with a limited number of array elements, while the size of the correlation matrix becomes greater than those from $MUSIC$ or $ROOT\text{-}MUSIC$ when large arrays are considered [26].

In order to reduce the computational costs as well as the risk of being trapped in false maxima of the LF, the data-supported optimization (DSO) can be suitably employed with $ESPRIT$ [18].

Such a procedure consists in partitioning the data sample in a large number of "*elemental sets*" for allowing a simpler computation of the estimates for each elemental data set. The advantages of such a technique have been widely demonstrated and exploited also in other application contexts [30]. The so-obtained values constitute a data-supported grid (DSG) over which the LF function is maximized.

Although eigenstructure-based approaches constitute the state-of-the-art in DoA estimation and demonstrated their optimality (as the best compromise between accuracy and computational load) in dealing with a limited number of incoming signals and/or limited number of receivers, unsatisfactory performances (i.e., with conspicuous differences compared to ML) occur in the so-called *threshold region*, namely, when the signal-to-noise ratio is low, or alternatively, when the number of snapshots is small.

In order to deal with these situations, this paper presents an hybrid approach called memory-based $ESPRIT$-like (M-DSO-$ESPRIT$). Following the guideline of the DSO-$ESPRIT$ [31], the proposed method considers an $ESPRIT$-based estimator for computing the DSG and a memory mechanism for enhancing the estimation accuracy thanks to the reallocation of the information acquired at the previous steps, which is used as *a-priori* knowledge for successive estimates.

The paper is organized as follows. In Section 2, the direction finding problem is mathematically formulated. The M-DSO-$ESPRIT$ method is described in Section 3 by focusing on its innovative features. Section 4 is devoted at presenting a set of selected numerical results in order to point out potentialities and limitations of the proposed approach. The comparison with state-of-the-art superresolution techniques, in terms of performance as well as computational cost, is reported. Finally, some conclusions are drawn (Section 5).

2. MATHEMATICAL FORMULATION

Let us consider a ULA of M equally-spaced sensors and L ($L < M$) uncorrelated narrow-band signals impinging at each time instant $t_s = t_0 + s \triangle t$, $s = 1, \ldots, S$, on the antenna with plane wavefronts from different directions, $\underline{\Theta}(t_s) = \{\theta_l(t_s); l = 1, \ldots, L\}$ (Figure 1). Moreover, let us indicate with $\underline{\mathbf{y}}(t_s) = \{y_m(t_s); m = 1, \ldots, M\}^T$ the *snapshot* (i.e., the collection of data samples at t_s) collected by the M sensors at each time instant [†]. Under the assumption that the number

[†] The superscripts T and H denote the transpose and conjugate transpose operation, respectively.

of available snapshots is equal to N ($N \geq L$), the receiver output $\underline{\underline{\mathbf{Y}}}(t_s)$ can be expressed, according to the matrix notation [17, 32], as follows

$$\underline{\underline{\mathbf{Y}}}(t_s) = \underline{\underline{\mathbf{A}}}[\underline{\Theta}(t_s)]\,\underline{\underline{\mathbf{X}}}(t_s) + \underline{\underline{\mathbf{E}}}(t_s)\,. \tag{1}$$

In particular, $\underline{\underline{\mathbf{Y}}}(t_s) = \left\{\underline{\mathbf{y}}(t_{s-N+n})\,;\, n = 1, \ldots, N\right\}$ is a complex matrix of $M \times N$ elements (i.e., $\underline{\underline{\mathbf{Y}}} \in \mathbb{C}^{M\times N}$), $\underline{\underline{\mathbf{X}}} \in \mathbb{C}^{L\times N}$ is the matrix of signal waveforms, and $\underline{\underline{\mathbf{A}}} \in \mathbb{C}^{M\times L}$ is the steering matrix given by

$$\underline{\underline{\mathbf{A}}}[\underline{\Theta}(t_s)] = \{\underline{\mathbf{a}}[\theta_l(t_s)]\,;\, l = 1, \ldots, L\} \tag{2}$$

being $\underline{\mathbf{a}}[\theta_l(t_s)] = \left\{e^{j(m-1)\frac{2\pi}{\lambda}d\sin[\theta_l(t_s)]};\, m = 1, \ldots, M\right\}^T$ the steering vector of the array towards the direction $\theta_l(t_s)$. Moreover, $\underline{\underline{\mathbf{E}}} \in \mathbb{C}^{M\times N}$ is related to the noise modeled by means of a stationary and ergodic complex-valued Gaussian process of zero-mean characterized by an assigned signal-to-noise ratio (SNR). Furthermore, the noise samples at the receivers, $e_m(t_s)$, $m = 1, \ldots, M$, $s \geq 1$, are assumed to be statistically independent.

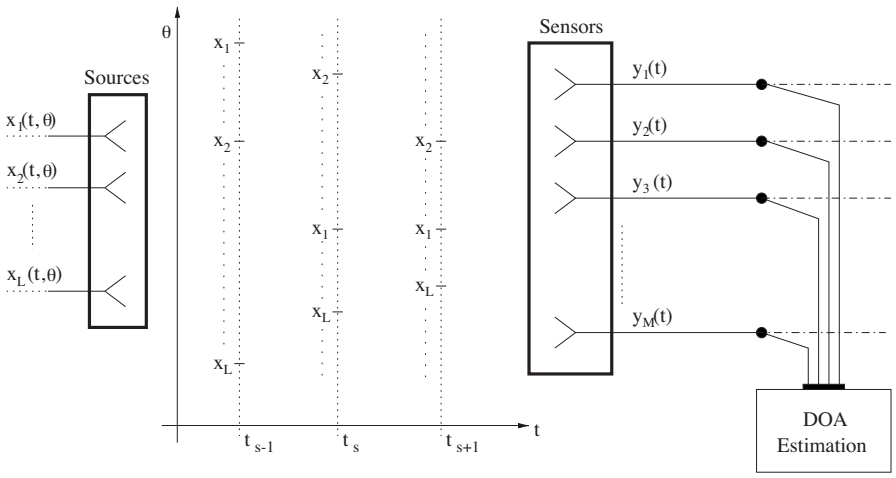

Figure 1. Problem geometry.

Under these hypotheses, the maximum likelihood localization of the L sources at t_s (i.e., the estimation of $\underline{\widehat{\Theta}}(t_s) = \{\widehat{\theta}_l(t_s)\,;\, l = 1, \ldots, L\}$) is obtained as [17, 32]

$$\underline{\widehat{\Theta}}(t_s) = \arg\max_{\underline{\Theta}(t_s)}\left[f_{ML}\left\{\underline{\Theta}(t_s)\right\}\right] \tag{3}$$

where f_{ML} is the likelihood function given by

$$f_{ML}\left\{\underline{\Theta}\left(t_s\right)\right\} = tr\left\{\underline{\underline{\mathbf{P}}}\left[\underline{\Theta}\left(t_s\right)\right]\underline{\underline{\mathbf{R}}}\left(t_s\right)\right\}. \tag{4}$$

and $tr\{\cdot\}$ indicates the trace of the matrix. Moreover,

$$\underline{\underline{\mathbf{P}}}\left[\underline{\Theta}\left(t_s\right)\right] = \underline{\underline{\mathbf{A}}}\left[\underline{\Theta}\left(t_s\right)\right]\left\{\underline{\underline{\mathbf{A}}}^H\left[\underline{\Theta}\left(t_s\right)\right]\underline{\underline{\mathbf{A}}}\left[\underline{\Theta}\left(t_s\right)\right]\right\}^{-1}\underline{\underline{\mathbf{A}}}^H\left[\underline{\Theta}\left(t_s\right)\right]$$

and

$$\underline{\underline{\mathbf{R}}}\left(t_s\right) = \frac{1}{N}\sum_{n=1}^{N}\underline{\mathbf{y}}\left(t_{s-N+n}\right)\underline{\mathbf{y}}^H\left(t_{s-N+n}\right)$$

are the *projection* and the *sample covariance* matrix [17], respectively.

Although the ML localization method allows one to obtain the optimal estimate, it usually requires the evaluation of the LF in correspondence with each possible combination of the DoAs. Such an event results in a computationally-expensive procedure, especially when dealing with multiple sources. Consequently, a suitable strategy aimed at optimizing the trade-off between localization accuracy and computational load could be advantageous. Towards this purpose, a new estimation technique is proposed in the following section.

3. THE M-DSO-ESPRIT METHOD

Unlike the optimal ML approach, the *M-DSO-ESPRIT* method resorts to the evaluation of the LF in a limited set of combinations of DoA and it considers a memory mechanism in order to fully exploit the acquired-knowledge (or *experience*) from previous estimates. More in detail, the following multi-step procedure is carried out at each time-step t_s, $s \geq 1$.

3.1. Memory Enhancement

The *M-DSO-ESPRIT* operates a memory enhancement of the collected data. Towards this end, a new memory-enhanced output matrix $\underline{\underline{\mathbf{D}}}\left(t_s\right)$

$$\underline{\underline{\mathbf{D}}}\left(t_s\right) = \left\{\underline{\mathbf{d}}_b\left(t_s\right);\, b = 1, \ldots, B\right\} \in \mathbb{C}^{M\times B}$$

is defined from the standard output matrix $\underline{\underline{\mathbf{Y}}}\left(t_s\right)$ as described in the following. At the first time-step ($s = 1$), the process is initialized by assuming $\underline{\underline{\mathbf{D}}}\left(t_1\right) = \underline{\underline{\mathbf{Y}}}\left(t_1\right)$, that is

$$\underline{\mathbf{d}}_b\left(t_1\right) = \underline{\mathbf{y}}\left(t_{s-N+b}\right) \quad b \in [1,\, B]\,; \quad B = N$$

otherwise ($s > 1$)

$$\underline{\mathbf{d}}_b(t_s) = \begin{cases} \underline{\mathbf{y}}(t_{s-N+b}) & b \in [1,\, N] \\ \underline{\mathbf{a}}\left[\widehat{\theta}_{b-N}(t_{s-1})\right] & b \in [N+1,\, B] \end{cases} \qquad B = N + L.$$

3.2. Data-Space Re-Sampling

The so-defined data space is then re-sampled. Starting from the matrix $\underline{\underline{\mathbf{D}}}(t_s)$ and considering the whole set of column combinations to obtain a matrix of dimension $M \times L$, it is possible to define K (being $K = \frac{B!}{L!(B-L)!}$) matrices $\underline{\underline{\mathbf{W}}}^{(k)} \in \mathbb{C}^{M \times L}$

$$\underline{\underline{\mathbf{W}}}^{(k)}(t_s) = \left\{ \underline{\mathbf{w}}_l^{(k)} = \underline{\mathbf{d}}_{c_l^{(k)}};\, l = 1, \ldots, L \right\} \quad k = 1, \ldots, K \tag{5}$$

where the index $c_l^{(k)} \in [1, B]$ identifies the column of $\underline{\underline{\mathbf{D}}}(t_s)$ corresponding to the l-th element of $\underline{\underline{\mathbf{W}}}^{(k)}(t_s)$, according to the iterative generation procedure detailed in Table 1. Moreover, in order to avoid wrong/unnecessary successive computations, the matrices whose condition numbers $\eta_s^{(k)}$ are greater than a fixed *stability threshold* (i.e., the ill-conditioned matrices) are omitted.

3.3. Data-Supported Grid Generation

As in [26, 31], an $ESPRIT$-like algorithm is used for generating the data-supported grid points. Let us consider the matrix $\underline{\underline{\Phi}}^{(k)} \in \mathbb{C}^{L \times L}$ given by

$$\underline{\underline{\Phi}}^{(k)}(t_s) = \left\{ \left[\underline{\underline{\mathbf{V}}}^{(k)}(t_s)\right]^H \underline{\underline{\mathbf{V}}}^{(k)}(t_s) \right\}^{-1} \left[\underline{\underline{\mathbf{V}}}^{(k)}(t_s)\right]^H \underline{\underline{\mathbf{U}}}^{(k)}(t_s) \tag{6}$$

where $\underline{\underline{\mathbf{V}}}^{(k)}$ and $\underline{\underline{\mathbf{U}}}^{(k)}$ are two matrices obtained from $\underline{\underline{\mathbf{W}}}^{(k)}$ by eliminating the first and last row, respectively. Then, the $ESPRIT$-like estimates (i.e., the K data-supported grid points) turn out to be

$$\underline{\widehat{\Theta}}^{(k)}(t_s) = \left\{ \hat{\theta}_l^{(k)}(t_s);\, l = 1, \ldots, L \right\} \qquad k = 1, \ldots, K \tag{7}$$

where $\hat{\theta}_l^{(k)} = \arcsin\left\{ \frac{\lambda}{2\pi d} \arg\left(\mu_l^{(k)}\right) \right\}$ and $\left\{ \mu_l^{(k)};\, l = 1, \ldots, L \right\}$ are the eigenvalues of $\underline{\underline{\Phi}}^{(k)}$ [29].

Table 1. Procedure for defining the matrices $\underline{\underline{\mathbf{W}}}^{(k)} \in \mathbb{C}^{M\times L}$, $k = 1, \ldots, K$.

```
k = 1
c_0^(k) = 0
for i = 1 , ..., L
      c_i^(k) = c_{i-1}^(k) + 1
end
go = TRUE
for k = 1 , ..., K
     for l = 1 , ..., L
          w_l^(k) = s_{c_l^(k)}
     end
     j = L
     while ({go} AND{j > 0}) then
          if c_j^(k) < B - L + j then
               c_j^(k+1) = c_j^(k) + 1
               if j < L then
                    for i = j + 1 , ..., L
                         c_i^(k+1) = c_{i-1}^(k+1) + 1
                    end
               end
               go = FALSE
          end
          j = j - 1
     end
end
```

3.4. *ML DoA* Estimation

Finally, the ML estimates of the DoAs of the L signals are computed by maximizing the LF over the K-sized data-supported grid:

$$\underline{\widehat{\Theta}}\,(t_s) = \arg \max_{\underline{\widehat{\Theta}}^{(k)}(t_s)} \left[f_{ML} \left\{ \underline{\widehat{\Theta}}^{(k)}\,(t_s) \right\} \right]. \tag{8}$$

4. NUMERICAL ASSESSMENT

The numerical assessment has been carried out by comparing the performances of the *M-DSO-ESPRIT* with those of other state-of-the-art approaches, such as *ROOT-MUSIC* [27], *ESPRIT* [29], *DSO-ESPRIT* [31] in order to point out its potentialities and current limitations as well as the range of convenient applicability. For completeness, the asymptotic performances achievable by an unbiased estimator of the parameters θ_l (i.e., the so-called Cramer-Rao bound (*CRB*) [33]) are reported, as well.

Concerning the estimation accuracy, the root-mean-square-error has been assumed as index of efficiency. Moreover, because of the statistical nature of the scenarios under test, its value averaged over $Q = 100$ independent realizations of each simulation has been computed

$$RMSE = \frac{1}{Q}\sum_{q=1}^{Q}\frac{1}{S}\sum_{s=1}^{S}\sqrt{\frac{1}{L}\sum_{l=1}^{L}\left|\theta_l^{(q)}(t_s) - \hat{\theta}_l^{(q)}(t_s)\right|^2} \tag{9}$$

where the index q denotes the q-th realization ($q = 1, \ldots, Q$) of a simulation, S being the total number of time-instants ($S = 100$).

As far as the reference antenna architecture is concerned, a linear array of $M = 20$ omnidirectional sensors $\frac{\lambda}{2}$-spaced has been adopted.

The first test case deals with "*stationary*" scenarios where L uncorrelated signals impinge from random, but fixed, directions [i.e., $\theta_l(t_s) = \theta_l$, $\forall s$]. Under this assumption, a set of experiments has been performed in order to show the effect of the size of the snapshot window (N), of the signal-to-noise ratio, and of the angular separation (i.e., $\triangle\theta_l = \theta_{l+1} - \theta_l$, $l = 1, \ldots, L-1$) between the *DoA*s of the sources on the method performances evaluated in terms of angular accuracy (i.e., *RMSE* value) and computational costs.

In the first experiment, the scenario under test is characterized by heavy noisy conditions ($SNR = 2\,\text{dB}$) and L sources coming from random angular directions equally-spaced by $\triangle\theta_l = 10°$, $l = 1, \ldots, L-1$. Under the assumption that $N = L$ (i.e., the minimum number of snapshots for a given configuration of sources), Figure 2 shows the behavior of the estimation error versus the number of sources L. Concerning the estimation accuracy, even though the resolution error is an increasing quantity, the *M-DSO-ESPRIT* outperforms the other direction finding methods and it results closer to the *CRB* when $L \leq 4$ pointing out a non-negligible robustness to the noise in localizing multiple sources. In order to quantify the computational cost, the amount of floating point operations needed at each time-

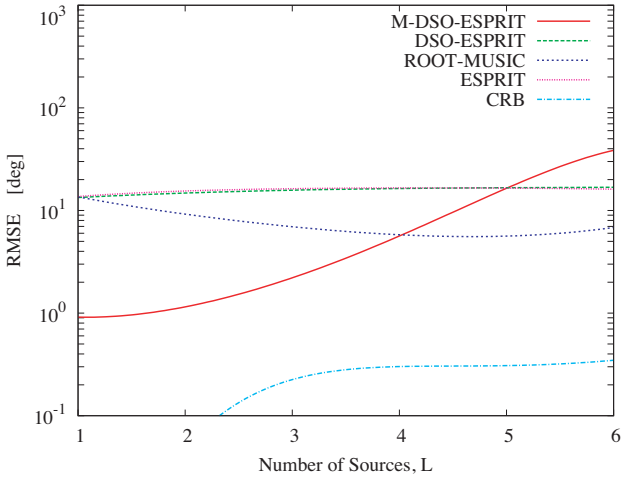

Figure 2. *Stationary Scenario* ($SNR = 2\,\mathrm{dB}$, $N = L$, $\triangle\theta_l = 10^\circ$, $\theta_1 = 10^\circ$) — $RMSE$ values versus number of sources L.

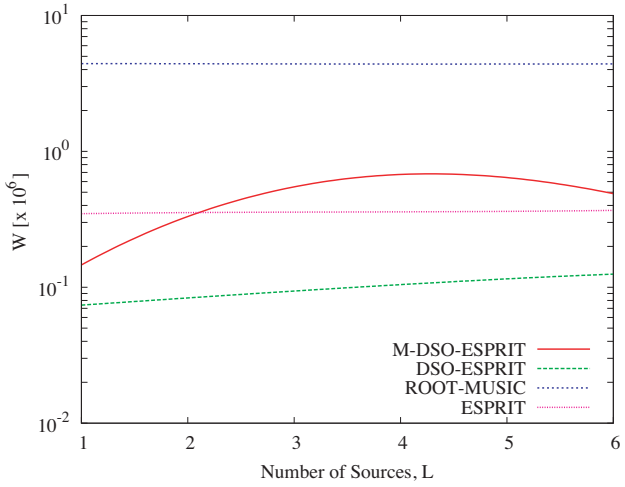

Figure 3. *Stationary Scenario* ($SNR = 2\,\mathrm{dB}$, $N = L$, $\triangle\theta_l = 10^\circ$, $\theta_1 = 10^\circ$) — Computational cost Ω versus number of sources L.

instant t_s (i.e., Ω) is analyzed (Figure 3). As expected, because of the memory enhancement and the dependence of the dimension of the output matrix $\underline{\underline{\mathbf{D}}}(t_s)$ on L, the computational burden required by *M-DSO-ESPRIT* grows with L, but not in a linear fashion since

the "*filtering*" procedure at the "*Data-Space Re-Sampling*" step avoids the processing of ill-conditioned matrices. Moreover, whatever the number of sources, the arising Ω value is greater than that of the *DSO-ESPRIT*, but of the same order in magnitude of the standard

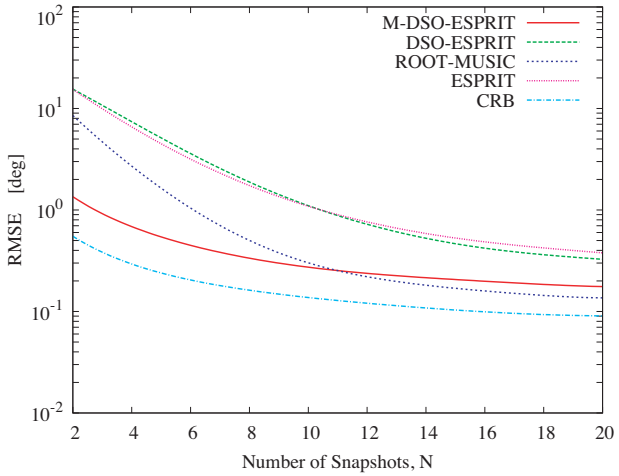

Figure 4. *Stationary Scenario* ($SNR = 2\,\mathrm{dB}$, $L = 2$, $\triangle\theta_l = 10°$, $\theta_1 = 10°$) — $RMSE$ values versus number of snapshots N.

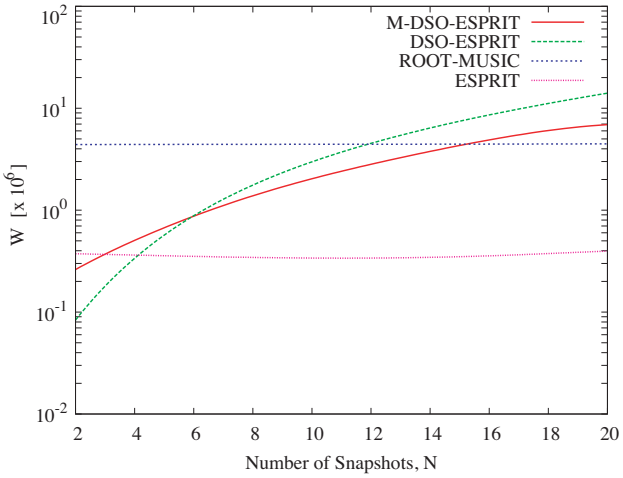

Figure 5. *Stationary Scenario* ($SNR = 2\,\mathrm{dB}$, $L = 2$, $\triangle\theta_l = 10°$, $\theta_1 = 10°$) — Computational cost Ω versus number of snapshots N.

ESPRIT. Furthermore, the *ROOT-MUSIC* technique results much more expensive in such a situation.

The second experiment is aimed at evaluating the behavior of the *M-DSO-ESPRIT* in correspondence with a variation of the number of snapshots. Towards this purpose, the scenario is the same of the first experiment, but the number of sources has been fixed to $L = 2$ (Figures 4 and 5) and $L = 4$ (Figures 6 and 7), respectively. Figures 4 and 6 show the resulted *RMSE* error as a function of N. As expected the statistical performances of the proposed estimator improve as N increases since the number of *DSO* grid points grows thus allowing the sampling of a larger portion of the entire *DoA* parameter space. Asymptotically, the estimation accuracy of the compared methods are quite similar to one another, but the *M-DSO-ESPRIT* confirms its effectiveness when operating in the *threshold region* when N is small.

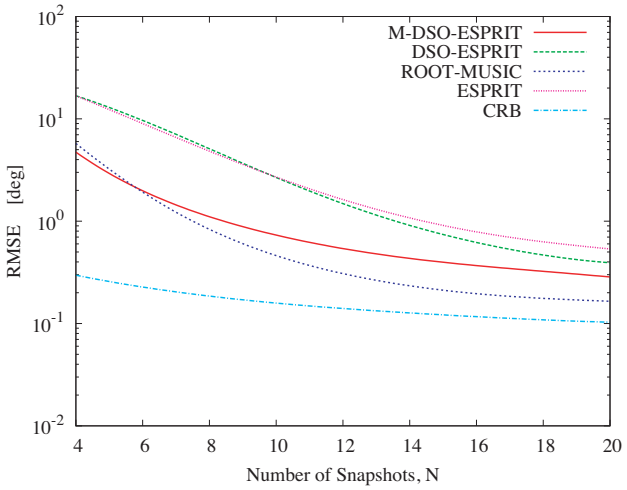

Figure 6. *Stationary Scenario* ($SNR = 2\,\text{dB}$, $L = 4$, $\triangle\theta_l = 10°$, $\theta_1 = 10°$) — *RMSE* values versus number of snapshots N.

On the other hand, unlike *ESPRIT* and *ROOT-MUSIC*, the computational burden required at each iteration by the *DSO*-based techniques depends on N. As a matter of fact, such approaches usually compute a number of *DoA* estimates equal to the number of combinations between the available temporal snapshots. Therefore, increasing the number of snapshots N involves a longer response time that could make the advantages in terms of resolution accuracy fruitless. Fortunately, the memory mechanism of the

M-DSO-ESPRIT positively acts allowing an evident (see Figure 7, $L = 4$) improvement over the *DSO-ESPRIT* in the critical (from a computational point of view) region (i.e., N large).

The third experiment deals with a scenario characterized by

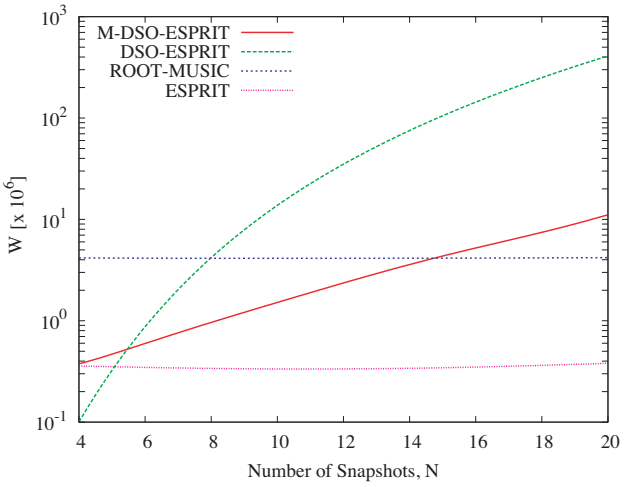

Figure 7. *Stationary Scenario* ($SNR = 2\,\mathrm{dB}$, $L = 4$, $\triangle\theta_l = 10°$, $\theta_1 = 10°$) — Computational cost Ω versus number of snapshots N.

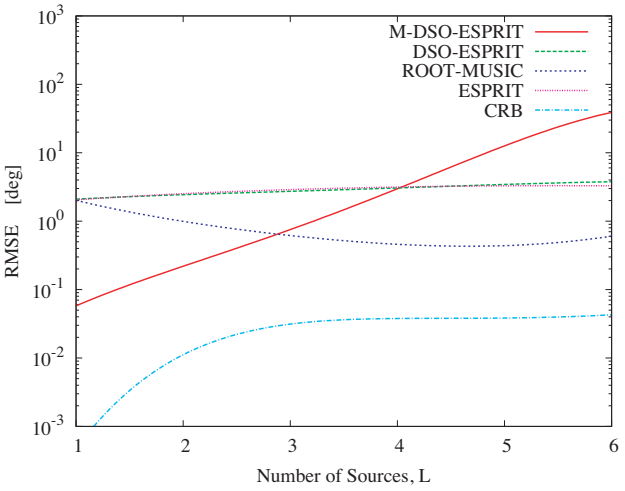

Figure 8. *Stationary Scenario* ($SNR = 20\,\mathrm{dB}$, $N = L$, $\triangle\theta_l = 10°$, $\theta_1 = 10°$) — $RMSE$ values versus number of sources L.

a better signal-to-noise ratio ($SNR = 20\,\mathrm{dB}$) in order to study the behavior of the memory-enhanced *DSO-ESPRIT* in a region outside (or only partially overlapped, when N is small) the *threshold region*. As expected, the *M-DSO-ESPRIT* appears to satisfactory perform for a limited number of sources ($L \leq 3$ — Figure 8). As a matter of fact, by keeping $L = 2$ and varying N (Figure 9), it asymptotically guarantees similar results to those of the other methods, while the *M-DSO-ESPRIT* significantly overcomes the standard *DSO-ESPRIT* implementation for small values of N ($\left.\frac{RMSE_{DSO\text{-}ESPRIT}}{RMSE_{M\text{-}DSO\text{-}ESPRIT}}\right|_{L=N=2} \cong 10$).

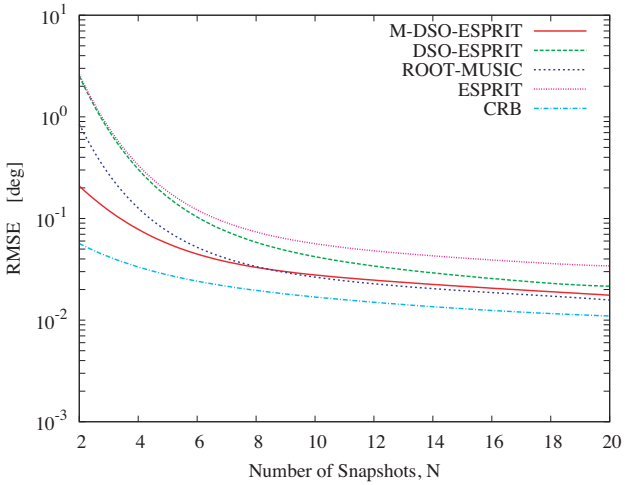

Figure 9. *Stationary Scenario* ($SNR = 20\,\mathrm{dB}$, $L = 2$, $\triangle\theta_l = 10°$, $\theta_1 = 10°$) — $RMSE$ values versus number of snapshots N.

The last set of experiments concerned with a "*stationary*" scenario is devoted at testing how the source separation affects the direction finding accuracy of the proposed approach. Figure 10 shows the root-mean-squared error values versus $\triangle\theta_l$ when $SNR = 2\,\mathrm{dB}$, $L = 2$ and $N = L$. As it can be observed, the *M-DSO-ESPRIT* performs quite well and close to the *CRB* when $\triangle\theta_l > 8°$. Moreover, an efficiency degradation verifies in correspondence with smaller separations ($\triangle\theta_l < 8°$), although a better resolution, compared to the other techniques, is always achieved. Similar conclusions on the comparative assessment hold true by varying the number of snapshots and keeping constant the angular separation to $\triangle\theta_l = 2°$ (Figure 11).

In order to qualitatively summarize the performance of the *M-DSO-ESPRIT* in terms of both estimation capabilities and

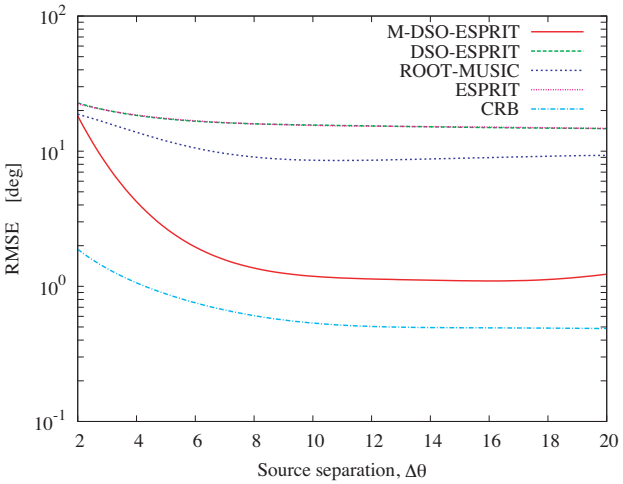

Figure 10. *Stationary Scenario* ($SNR = 2\,\mathrm{dB}$, $L = 2$, $N = L$, $\theta_1 = 10°$) — $RMSE$ values versus source separation distance $\Delta\theta$.

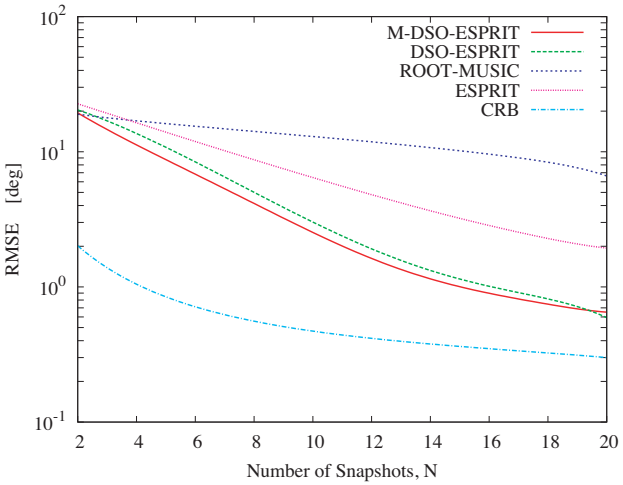

Figure 11. *Stationary Scenario* ($SNR = 2\,\mathrm{dB}$, $L = 2$, $\triangle\theta_l = 2°$, $\theta_1 = 10°$) — $RMSE$ values versus number of snapshots N.

computational costs when dealing with *stationary* conditions, Table 2 pictorially resumes the behavior of the approach versus the number of sources L (1: many, 0: few), the number of snapshots N (1: many — $N > L$, 0: few — $N = L$), the angular source separation $\Delta\theta$

(1: large, 0: small), and the SNR (1: low level of noise, 0: high level of noise). According to the indications drawn from the numerical experiments, Table 2 points out and confirms that the approach is an effective alternative to standard estimators especially in the *threshold region* defined by a low SNR or/and a small number of snapshots.

Table 2. *Stationary Scenario* — Summary of the *M-DSO-ESPRIT* performances.

L	N	$\Delta\theta$	SNR	*RMSE*	Ω
0	0	0	0	☺	☺
0	0	0	1	☺	☺
0	0	1	0	☺	☺
0	0	1	1	☺	☺
0	1	0	0	☺	☹
0	1	0	1	☺	☹
0	1	1	0	☺	☹
0	1	1	1	☺	☹
1	0	0	0	☹	😐
1	0	0	1	😐	😐
1	0	1	0	😐	😐
1	0	1	1	☹	😐
1	1	0	0	☹	☹
1	1	0	1	☺	☹
1	1	1	0	☺	☹
1	1	1	1	😐	☹

The second test case is concerned with a complex environment characterized by the time-variance of the randomly-distributed *DoA*s of the impinging signals. Figure 12(a) pictorially describes the scenario under test characterized by $L = 3$ sources having a variable direction of incidence $[\theta_l(t_s) \in [-40°, 50°]; l = 1, \ldots, L; s = 1, \ldots, S; S = 60]$. As far as the estimation process is concerned, $N = 3$ snapshots have been considered and different noisy conditions have been simulated (i.e., $SNR = 2\,\text{dB}$, $SNR = 10\,\text{dB}$, and $SNR = 20\,\text{dB}$).

The achieved performances in terms of $RMSE$ are shown in Figure 12 and detailed in Table 3. As expected, when dealing with the case of $SNR = 2\,\text{dB}$, the *M-DSO-ESPRIT* usually achieves the best accuracy in the estimates [Figure 12(b)] as confirmed by comparing the mean (over the complete temporal window of $S = 60$ time-steps)

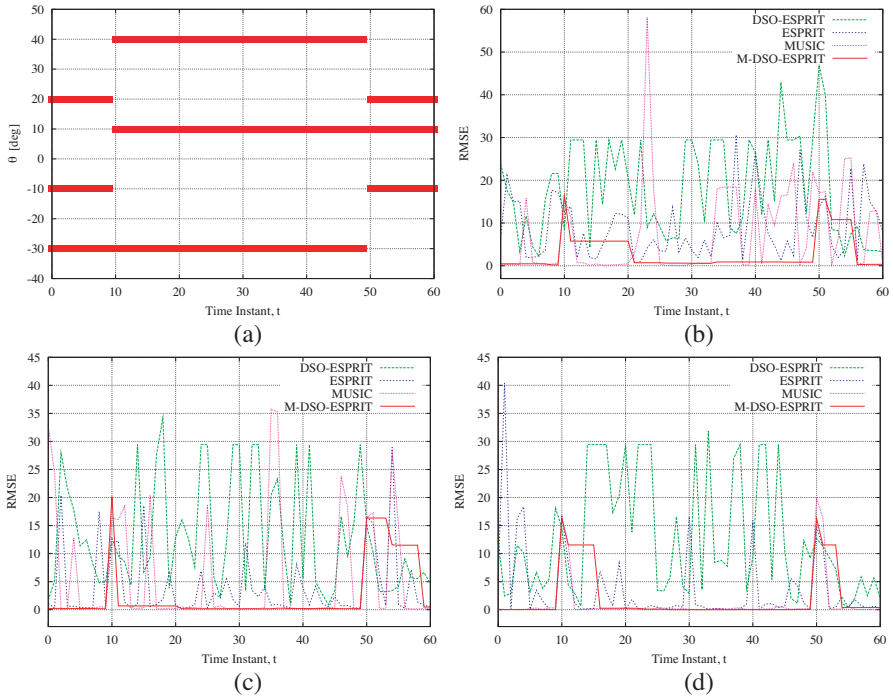

Figure 12. *Time-Varying Scenario* ($L = 3$, $N = L$, $\theta_l(t_s) \in [-40°, 50°]$, $S = 60$). (a) Reference configuration. $RMSE$ at each t_s, $s = 1, \ldots, S$ when (b) $SNR = 2\,\text{dB}$, (c) $SNR = 10\,\text{dB}$, and (d) $SNR = 20\,\text{dB}$.

values of the $RMSE$ in Table 3 ($\varsigma_{RMSE}^{M\text{-}DSO\text{-}ESPRIT} = 4.45\big\rfloor_{SNR=2\,\text{dB}}$ vs. $\varsigma_{RMSE}^{ROOT\text{-}MUSIC} = 8.59\big\rfloor_{SNR=2\,\text{dB}}$, $\varsigma_{RMSE}^{ESPRIT} = 12.29\big\rfloor_{SNR=2\,\text{dB}}$, and $\varsigma_{RMSE}^{DSO\text{-}ESPRIT} = 12.21\big\rfloor_{SNR=2\,\text{dB}}$). Concerning the scenario characterized by $SNR = 10\,\text{dB}$, the reliability of *M-DSO-ESPRIT* is significantly better than those of *ESPRIT* and *DSO-ESPRIT* [Figure 12(c) — Table 3] ($\varsigma_{RMSE}^{M\text{-}DSO\text{-}ESPRIT} = 2.94\big\rfloor_{SNR=10\,\text{dB}}$ vs. $\varsigma_{RMSE}^{ESPRIT} = 6.63\big\rfloor_{SNR=10\,\text{dB}}$, $\varsigma_{RMSE}^{DSO\text{-}ESPRIT} = 6.59\big\rfloor_{SNR=10\,\text{dB}}$) and it also overcomes the performance of *ROOT-MUSIC* ($\varsigma_{RMSE}^{ROOT\text{-}MUSIC} = 3.59\big\rfloor_{SNR=10\,\text{dB}}$). Such an event is mostly due to the fast "reaction" of the *M-DSO-ESPRIT* to the scenario variations in correspondence with the time-step transitions (i.e., $t_s = 10, 50$). Finally [$SNR = 20\,\text{dB}$ — Figure 12(d)], despite the lower noise level and although there is a slight improvement in the estimation accuracy with the increasing of SNR ($\varsigma_{RMSE}^{M\text{-}DSO\text{-}ESPRIT}\big\rfloor_{SNR=10\,\text{dB}} =$

2.94 vs. $\varsigma_{RMSE}^{M\text{-}DSO\text{-}ESPRIT}\big|_{SNR=20\,\mathrm{dB}} = 2.82$), the *M-DSO-ESPRIT* does not reach the effectiveness of the *ROOT-MUSIC* approach ($\varsigma_{RMSE}^{ROOT\text{-}MUSIC}\big|_{SNR=20\,\mathrm{dB}} = 1.96$). On the other hand, it should be noticed that, whatever the noise level, the memory-enhanced version of the *DSO-ESPRIT* always overcomes the standard implementation ($\frac{\varsigma_{RMSE}^{DSO\text{-}ESPRIT}}{\varsigma_{RMSE}^{M\text{-}DSO\text{-}ESPRIT}}\Big|_{SNR=2\,\mathrm{dB}} \cong 2.74$, $\frac{\varsigma_{RMSE}^{DSO\text{-}ESPRIT}}{\varsigma_{RMSE}^{M\text{-}DSO\text{-}ESPRIT}}\Big|_{SNR=10\,\mathrm{dB}} \cong 2.24$, and $\frac{\varsigma_{RMSE}^{DSO\text{-}ESPRIT}}{\varsigma_{RMSE}^{M\text{-}DSO\text{-}ESPRIT}}\Big|_{SNR=20\,\mathrm{dB}} \cong 1.19$).

Table 3. *Time-Varying Scenario* ($L = 3$, $N = L$, $\theta_l(t_s) \in [-40°, 50°]$, $S = 60$). Time-averaged values of the $RMSE$.

	SNR [dB]		
	2	10	20
M-DSO-ESPRIT	4.45	2.94	2.82
DSO-ESPRIT	12.21	6.59	3.37
ESPRIT	12.29	6.63	3.31
ROOT-MUSIC	8.59	3.59	1.96

5. CONCLUSIONS

In this paper, a *DoA* estimation method has been proposed in order to deal with complex scenarios belonging to the so-called *threshold region*, thus improving the effectiveness of direction finding techniques and extending their range of applicability. Starting from a simple and computationally-efficient data supported optimization for the solution of the maximum likelihood estimation problem, a memory mechanism has been introduced. The approach, called *M-DSO-ESPRIT*, increases the number of the data-supported samples, over which the likelihood function is maximized, by extending the data set with the maximum likelihood estimates of the previous time-steps.

Concerning the main features of the *M-DS-ESPRIT*, they can be summarized as follows

- effective exploitation of the information acquired during the estimation process;
- computational simplicity in comparison with optimal approaches.

As far as the numerical validation and the comparative study with other state-of-the-art methods are concerned, the obtained results demonstrated the efficiency of the proposed approach in terms of both estimation accuracy and computational burden, especially in those scenarios where

- the environmental conditions heavily affect the signal-to-noise ratio;
- the number of collectable snapshots is limited.

On the other hand, it cannot be neglected that the *M-DSO-ESPRIT* guarantees acceptable performances also in the presence of low levels of noise or when longer temporal windows are considered, thus indicating the flexibility of the method.

Future works will be devoted at experimentally validating the memory-based *DSO-ESPRIT* technique as well as improving its effectiveness in facing with fast time-varying scenarios.

ACKNOWLEDGMENT

This work has been supported in Italy by the "Progettazione di un Livello Fisico 'Intelligente' per Reti Mobili ad Elevata Riconfigurabilità" Progetto di Ricerca di Interesse Nazionale — MIUR Project COFIN 2005099984.

REFERENCES

1. Alexiou, A. and M. Haardt, "Smart antenna technologies for future wireless systems: Trends and challenges," *IEEE Commun. Mag.*, Vol. 42, No. 9, 90–97, 2004.
2. Fakoukakis, F. E., S. G. Diamantis, A. P. Orfanides, and G. A. Kyriacou, "Development of an adaptive and a switched beam smart antenna system for wireless communications," *Journal of Electromagnetic Waves and Applications*, Vol. 20, No. 3, 399–408, 2006.
3. Wu, W., B. Z. Wang, and S. Sun, "Pattern reconfigurable microstrip patch antenna," *Journal of Electromagnetic Waves and Applications*, Vol. 19, No. 1, 107–113, 2005.
4. Ragheb, M. K., S. H. Elramly, and S. Mostafa, "The effect of varying the input parameters on the performance capabilities of three different doa estimation algorithms using smart antennas," *Proc. 20th National Radio Sci. Conf.*, 1–9, March 2003.

5. Varlamos, P. K. and C. N. Capsalis, "Electronic beam steering using switched parasitic smart antenna arrays," *Progress In Electromagnetics Research*, PIER 36, 101–119, 2002.
6. Wu, W. and Y. H. Bi, "Switched-beam planar fractal antenna," *Journal of Electromagnetic Waves and Applications*, Vol. 20, No. 3, 409–415, 2006.
7. Mouhamadou, M., P. Vaudon, and M. Rammal, "Smart antenna array patterns synthesis: Null steering and multi-user beamforming by phase control," *Progress In Electromagnetics Research*, PIER 60, 95–106, 2006.
8. Mukhopadhyay, M., B. K. Sarkar, and A. Chakrabarty, "Augmentation of anti-jam Gps system using smart antenna with a simple DoA estimation algorithm," *Progress In Electromagnetics Research*, PIER 67, 231–249, 2007.
9. Babayigit, B., A. Akdagli, and K. Guney, "A clonal selection algorithm for null synthesizing of linear antenna arrays by amplitude control," *Journal of Electromagnetic Waves and Applications*, Vol. 20, No. 8, 1007–1020, 2006.
10. Gavan, J. and J. S. Ishay, "Hypothesis of natural radar tracking and communication direction finding systems affecting hornets flight," *Progress In Electromagnetics Research*, PIER 34, 299–312, 2001.
11. Saka, B., E. Afacan, and E. Yazgan, "Beam steering antenna design for low altitude radar systems," *Journal of Electromagnetic Waves and Applications*, Vol. 11, No. 2, 215–224, 1997.
12. Paine, A. S., "Fast MUSIC for large 2-D element digitised phased array radar," *Proc. Int. Radar Conf. 2003*, 200–205, September 2003.
13. Owsley, N. L., "Sonar array processing," *Array Signal Processing*, S. Haykin (ed.), 115–193, Prentice-Hall, Englewood Cliffs, NJ, 1984.
14. Nishiura, T. and S. Nakamura, "Talker localization based on the combination of DOA estimation and statistical sound source identification with microphone array," *IEEE Workshop Statistical Signal Processing 2003*, 597–600, October 2003.
15. Schweppe, F. C., "Sensor array data processing for multiple signal sources," *IEEE Trans. Inform. Theory*, Vol. 14, 294–305, 1968.
16. Stoica, P., R. L. Moses, B. Friedlander, and T. Söderström, "Maximum likelihood estimation of the parameters of multiple sinusoids from noisy measurements," *IEEE Trans. Acoust., Speech, Signal Processing*, Vol. 37, 378–392, 1989.

17. Ziskind, I. and M. Wax, "Maximum likelihood localization of multiple sources by alternating projection," *IEEE Trans. Acoust., Speech, Signal Process.*, Vol. 36, 1553–1560, 1988.
18. Stoica, P. and A. B. Gershman, "Maximum-likelihood *DoA* estimation by data-supported grid search," *IEEE Signal Processing Lett.*, Vol. 6, No. 10, 273–275, 1999.
19. El-Zooghby, A. H., C. G. Christodoulou, and M. Georgiopoulos, "Performance of radial-basis function network for direction arrival estimation with antenna arrays," *IEEE Trans. Antennas Propagat.*, Vol. 45, 1611–1617, 1997.
20. El-Zooghby, A. H., C. G. Christodoulou, and M. Georgiopoulos, "A neural network-based smart antenna for multiple source tracking," *IEEE Trans. Antennas Propagat.*, Vol. 48, 768–776, 2000.
21. Pastorino, M. and A. Randazzo, "A smart antenna system for direction of arrival estimation based on a support vector regression," *IEEE Trans. Antennas Propagat.*, Vol. 53, No. 7, 2161–2168, 2005.
22. Donelli, M., R. Azaro, L. Lizzi, F. Viani, and A. Massa, "A SVM-based multi-resolution procedure for the estimation of the DOAs of interfering signals in a communication system," *Proc. European Conference Antennas Propagat. (*EuCAP*)*, 363898, Nice, France, November 2006.
23. Pastorino, M. and A. Randazzo, "The SVM-based smart antenna for estimation of the directions of arrival of electromagnetic waves," *IEEE Trans. Intrum. Meas.*, Vol. 55, No. 6, 1918–1925, 2006.
24. Schmidt, R. O., "Multiple emitter location and signal parameter estimation," *IEEE Trans. Antennas Propagat.*, Vol. 34, No. 3, 276–280, 1986.
25. Godara, L. C., "Application of antenna arrays to mobile communications, part II: Beam-forming and direction-of-arrival considerations," *IEEE Proc.*, Vol. 85, No. 8, 1195–1245, 1997.
26. Al-Ardi, E. M., R. M. Shubair, and M. E. Al-Mualla, "Investigation of high resolution DoA estimation algorithms for optimal performance of smart antenna systems," *Proc. 4th Int. Conf. 3G Mobile Comm. Technol.*, 460–464, June 2003.
27. Barabell, A., "Improving the resolution of eigenstructured based direction finding algorithms," *IEEE Proc. ICASSP'83*, Vol. 8, 336–339, April 1983.
28. Rao, B. D. and K. V. S. Hari, "Performance analysis of root-

music," *IEEE Trans. Acoust., Speech, Signal Process.*, Vol. 37, No. 12, 1939–1949, 1989.

29. Roy, R. and T. Kailath, "ESPRIT — Estimation of signal parameters via rotational invariance techniques," *IEEE Trans. Acoust., Speech, Signal Process.*, Vol. 37, No. 7, 984–995, 1989.
30. Hawkins, D. M., D. Bradu, and G. V. Kass, "Location of several outliers in multiple regression data using elemental sets," *Thechnometrics*, Vol. 26, 197–208, 1984.
31. Gershman, A. B. and P. Stoica, "Data-supported optimization for maximum likelihood DoA estimation," *IEEE Proc. SAMSP'00*, 337–341, March 2000.
32. Stoica, P. and K. C. Sharman, "Maximum likelihood methods for direction-of-arrival estimation," *IEEE Trans. Acoust., Speech, Signal Process.*, Vol. 38, 1132–1143, 1990.
33. Stoica, P. and A. Nehorai, "Music, maximum likelihood, and Cramer-Rao bound," *IEEE Trans. Acoust., Speech, Signal Process.*, Vol. 37, No. 5, 720–741, 1989.